Supplementary information

Layer-by-layer assembly of multi-layered droplet interface bilayers (multi-DIBs)

Matthew E. Allen‡, James Albon‡ and Yuval Elani*

Materials and methods

Materials

The lipids 1-palmitoyl-2-oleoyl-*sn*-glycero-3-phosphocholine (POPC), 1,2-dioleoyl-sn-glycero-3-phosphoethanolamine-N-(7-nitro-2-1,3-benzoxadiazol-4-yl) (ammonium salt) (NBD-PE), 1,2-dioleoyl-sn-glycero-3-phosphoethanolamine-N-(lissamine rhodamine B sulfonyl) (ammonium salt) (Rh-PE) and 1,2-dioleoyl-sn-glycero-3-phosphoethanolamine-N-(Cyanine 5) (Cy5-PE) were purchased from Avanti Polar lipids (USA). Both Mineral oil and Silicone oil AR 200 were purchased from Sigma Aldrich (UK). All other reagents (Glucose, Maltotriose, Calcein, HEPES, Cobalt (II) 2-ethyhexanoate) were purchased from Sigma Aldrich (UK).

Production of trilayer droplets

Lipid films were initially produced by depositing POPC lipid dissolved in chloroform within a glass vial before removing the chloroform under a gentle stream of N_2. The vial was then placed in a lyophiliser overnight to remove any residual chloroform. The dried lipid films then had appropriate amounts of Silicone and Mineral oil added to them to produce 2mg ml^{-1} lipid in oil solutions. To ensure the lipids were fully dissolved in the oil solutions, they were sonicated for 30 minutes at 50°C. For experiments where fluorescent lipids were used the lipid films had 1 mol % of the relevant fluorescent lipid included in them. All aqueous solutions were prepared by dissolving the appropriate masses in deionised water.

In order to form the trilayer droplets, a column was first prepared in an Eppendorf where 300μl of 0.5M Glucose was pipetted over 300μl of lipid in Silicone oil to form a water/ oil column. 100μl of lipid in Mineral oil was then pipetted over the top of this column to create a final oil/water/oil column with two interfaces where the lipids assemble into a monolayer due to their amphiphilic nature. This was left to settle for 2 hours to enable efficient lipid monolayer assembly at the oil/water interfaces. Each layer in the column had a different density (Silicone oil - ρ=1.05 g ml^{-1}, 0.5M Glucose - ρ=1.03 g ml^{-1} and Mineral oil - ρ=0.84 g ml^{-1}), this enabled the column to assemble in the correct order (by density) and allowed a larger density substance to travel through all of the interfaces to collect at the bottom of the Silicone oil.

An emulsion was then created by mixing 40μl of the 0.5M Maltotriose solution with 200μl of lipid in Mineral oil. The Maltotriose solution had a density of ρ=1.09 g ml^{-1} (larger than all of the densities in the column) to facilitate the droplets falling through the entirety of the column. The solution was mixed through pipetting up and down 20 times, this coated the cell-sized Maltotriose droplets with a single monolayer. The emulsion was then pipetted over the created column. The column was then centrifuged for 10 minutes at 9000g to form a pellet at the bottom of the Eppendorf.

The driving of the dense monolayer coated Maltotriose droplets through the column forced the droplets through both oil/ water interfaces where another monolayer was picked up at each interface resulting in final droplets that had had 3 monolayers deposited upon them, thus forming a trilayer structure. The centrifugation step also initiates stochastic collisional based contact between the individual trilayer droplets to form the multi-layered DIBs. All of the supernatant was extracted before fresh Mineral oil was added to the pellet. The pellet was then resuspended by pipetting up and down 10 times.

Imaging of trilayer droplets and multi-layered DIBs

The trilayer droplets were imaged by placing the Mineral oil solution in a PDMS spacer on a microscopy slide. A cover slip was then placed on top of the PDMS spacer to seal the sample chamber. Droplets were visualised on a Nikon eclipse Ti2-U inverted microscope with a CoolLED pE-300[white] and a Nikon DS-Qi2 camera. For fluorescence imaging FITC, TRITC and Cy5 filter cubes were used to image NBD, Rhodamine and Cy5 dyes respectively.

To produce the DIBs comprised of trilayer and monolayer coated droplets. A collection of trilayer droplets were mixed with an emulsion generated from pipetting 20µL of 0.5M Maltotriose with 200µL of Mineral oil stabilised by 2mg ml^{-1} of POPC. The resulting solution was mixed well through manual pipetting before being imaged.

Production and imaging of single bilayer DIBs

Single bilayer DIBs were constructed using the standard lipid out protocol. POPC lipid dissolved in chloroform was deposited within a glass vial before the chloroform was removed under a gentle stream of N$_2$. The resultant film was lyophilised overnight to remove the residual chloroform. The lipid was then dissolved in Mineral oil through 30 minutes of sonication at 50°C to form a 10 mg ml^{-1} lipid in oil solution. 100µl of the lipid containing Silicone/Mineral oil solution then filled a PDMS well on a PDMS coated glass slide. 0.5µL of 0.5M Maltotriose solution was then injected into the PDMS wells forming aqueous droplets within the oil. For asymmetric DIB production the volume injected for each of the droplets varied slightly from this central value. E.g., 0.45 and 0.55µL. The droplets were left to stabilise for 30 minutes before being pushed together with a needle to form DIBs. After the DIBs had equilibrated for 30 minutes images were taken on a Nikon Eclipse TE2000-E inverted microscope using a Ximea MQ013MG-E2 camera.

Fluorescence quenching experiments

For the fluorescence quenching experiments, the central monolayer (the Mineral oil phase in the phase transfer column) contained 1 mol% NBD-PE in the 2 mg ml^{-1} lipid film used. The control experiments additionally had 0.5 mol% Cobalt (II) 2-ethylhexanoate within the NBD-PE containing Mineral oil in the phase transfer column. The NBD-PE within the trilayer droplets were visualised on a Nikon Eclipse TE2000-E inverted microscope using a Ximea MQ013MG-E2 camera, a mercury arc lamp and a FITC filter. For the regular experiments the quencher was added after an initial NBD fluorescence image was taken. As a consequence, the sample then contained an overall concentration of 0.5 mol% of the quencher before further

fluorescent imaging occurred. The obtained fluorescent images were then normalised using the following equation to minimise the impact of background fluorescence.

$$Normalised\ fluorescence\ to\ background = \frac{Droplet\ intenstiy\ -\ Background\ intensity}{Background\ intensity}$$

(**Equation S1**)

Fluorimetry

Fluorimetry experiments were carried out on a Cary Eclipse Fluorescence Spectrophotometer (Agilent, Santa Clara, USA) in black, 40 μl volume 384 well-plates (Dow Corning, Midland, USA). 1 mol % Cobalt (II) 2-ethylhexanoate in Mineral oil was added to NBD labelled 2 mg ml^{-1} lipids in Mineral oil solutions to form an overall quencher concentration of 0.5 mol %.

Fluorescence recovery after photobleaching (FRAP) of Calcein containing multi-DIBs

The multi-layered droplets used for FRAP were prepared by the same general protocol as before however the 0.5M Maltotriose solution also contained 10mM of HEPES buffer (pH 7.4) and 50μM of Calcein solution.

A Leica TSC SP5 inverted confocal microscope was used to perform the FRAP experiments where the Calcein fluorescence within the multi-DIBs were imaged using an Argon laser (excitation 488nm) with emission collected from 500- 600nm. Samples were imaged at 20% laser power for 10 minutes (at 30s intervals) to collect pre bleach data. The samples were then bleached by applying 100% laser power to a single droplet continuously for 5 minutes. After bleaching, the sample was imaged at 20% laser power for 60 minutes (at 30s intervals). To normalise the fluorescence of each sample equation S2 was used. F was the fluorescence at a given time point in the photobleached droplet, $F_{pre\ bleach}$ was the maximum fluorescence intensity before photobleaching in the droplet while $F_{initial\ post\ bleach}$ was the fluorescence intensity immediately after photobleaching in the droplet.

$$Normalised\ fluorescence = \frac{(F - F_{initial\ post\ bleach})}{(F_{pre\ bleach} - F_{initial\ post\ bleach})}$$

(**Equation S2**)

Supplementary notes

Oil retention

The protocol developed to produce the trilayer coated droplets has relied on the utilisation of the inverted emulsion method. As this method has been used extensively to produce Giant Unilamellar Vesicles (GUVs) the retention of oil within the leaflet of the GUV bilayer has been investigated by others. It has been seen that the bending rigidities of the inverted emulsion formed GUVs did not differ significantly from GUVs formed from electroformation (a non-oil containing method of

GUV generation)[1] and that GUVs produced from the inverted emulsion method are free enough from oil to enable membrane protein insertion[2]. Furthermore, other work carried out to produce multi membrane GUVs[3] has shown that the addition of further templated bilayers linearly scaled the bending rigidity of the system indicating that oil was not significantly impacting the multilayered GUV properties. These results indicate that even if there is residual oil present, it is not in large enough quantities to impact the properties of the inner and central leaflets of the produced trilayer.

However, DIB systems have been shown to be impacted by the composition of the external oil[4] although many DIB systems can readily incorporate transmembrane proteins[5,6], show formation of lipid domains across the bilayer[7] and present similar bilayer capacitances to oil free membranes[8], features which indicate the space between the two outer leaflets is virtually 'oil free' and has negligible impact upon biological functionality.

Therefore, we would expect within our system that only the composition of the external oil will influence the properties of the outer leaflet of the trilayer droplets, and the multi-DIBs produced. However, we expect this to have no impact upon the biological functionality. Moreover, as centrifugation is utilised to pellet the trilayer droplets before resuspension into the final oil solution, the external oil composition can be readily changed to mitigate the impact of oil if required.

Supporting figures and equations
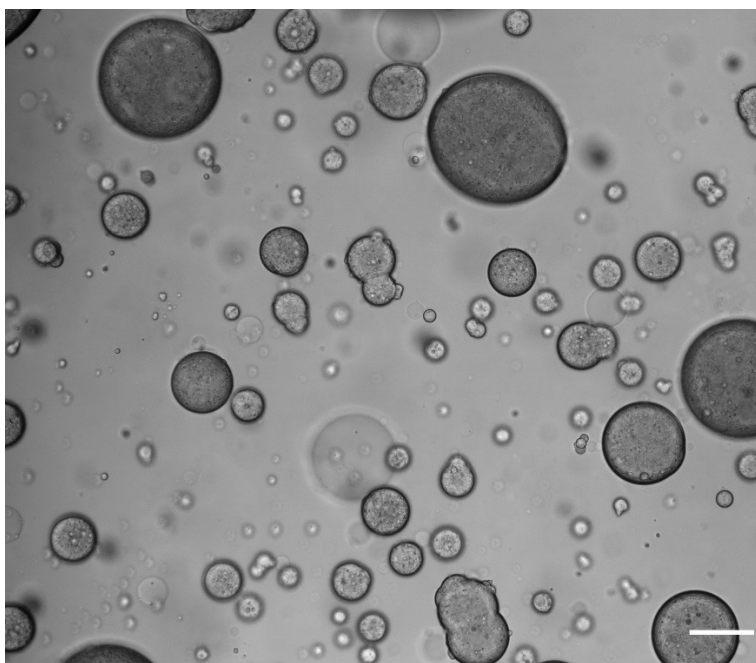
Figure S1: Representative brightfield image of a population of trilayer stabilised droplets and triple bilayer multi-DIBs. The scale bar is 50 microns. The deformation of some droplets is thought to occur through their interactions with the surface of the hydrophilic microscopy slide. The wetting of trilayer droplets to the glass slide can be reduced through coating the slides with Rain-X or PDMS to make the slides more hydrophobic and alter the energies between the slide and the trilayer droplets.
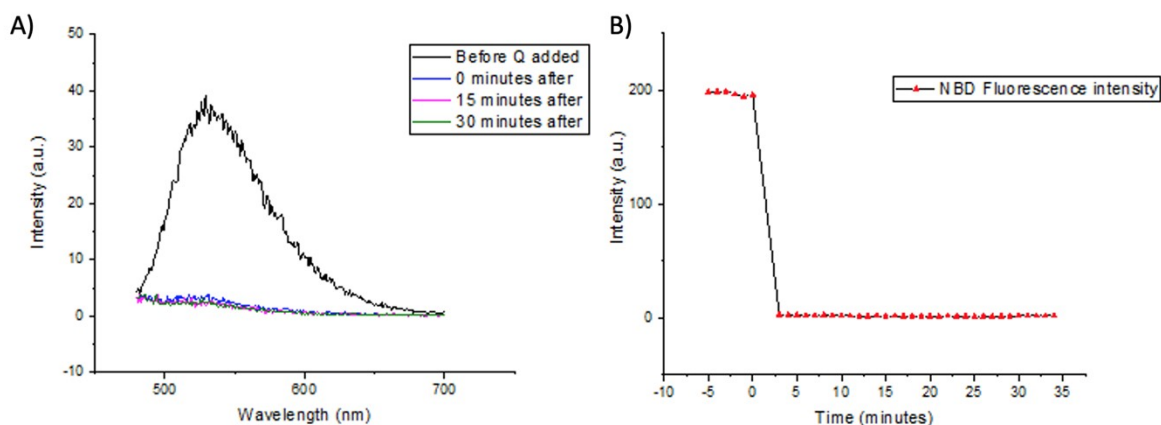
Figure S2: Kinetics of the Cobalt (II) 2-ethyhexanoate quencher in Mineral oil A) The impact of 0.5 mol% Cobalt quencher on the emission spectra of 2mg ml^{-1} NBD-PE in Mineral oil over time. B) The kinetics of quenching the NBD-PE emission spectra at 536 nm with 0.5 mol% of Cobalt quencher in Mineral oil. Both graphs indicate that within Mineral oil, the quenching of NBD-PE fluorescence occurs on a short (seconds) timescale.
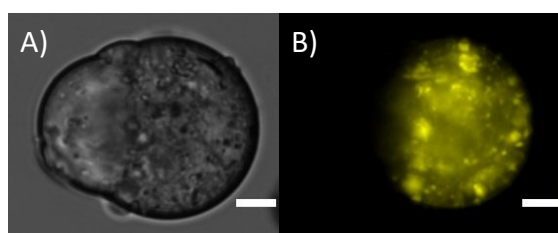
Figure S3: Confirmation of double bilayer production. A trilayer coated droplet labelled with Rhodamine-PE lipids contacted a monolayer coated droplet with no fluorescent tag. The resulting multi-DIB structure shows a clear divide between the trilayer and monolayer stabilised compartments through brightfield optical texture (A) and fluorescent labelling (B).

Contact angle analysis

Experimental images of both the multi-layered and single bilayer DIBs with asymmetric volumes within the constituent droplets were passed through a custom python script using the scikit image library that detected the constituent droplets that comprised the DIBs through binary thresholding and then a Hough transform. From the circles produced by the Hough transform both the radii (r_1 and r_2) and the centres ((x_1, y_1) and (x_2, y_2)) of the individual droplets could be obtained. These parameters were then used to calculate the contact angle of the DIBs. These parameters are also depicted within figure S4.
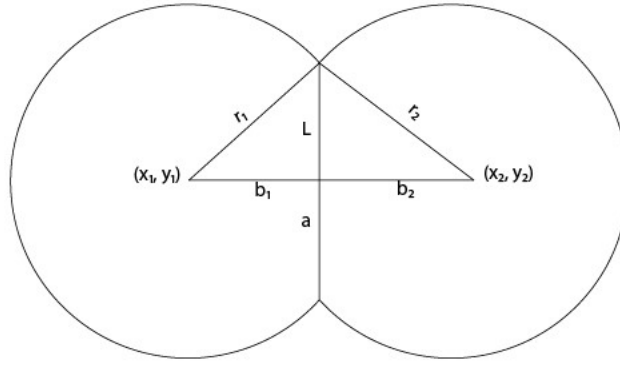
Figure S4: The geometrical parameters of a DIB.

To obtain an equation to describe the contact angle for asymmetric volume DIBs, the following derivation was applied to produce equations S9 and S10.

The DIB structure can be described as having the following geometrical properties as shown within figure S4 which give rise to equations S3-5. Here r_1 and r_2 are droplet radii, (x_1,y_1) and (x_2,y_2) are the centre points of each droplet, a is the droplet intersection radius and b_1 and b_2 are the distances from the droplet intersection radius to the centre of each droplet. b_1 and b_2 can also be summed up to produce d, the distance between the droplet centres.

$$a^2 + b_1^2 = r_1^2$$

(**Equation S3**)

$$a^2 + b_2^2 = r_2^2$$

(**Equation S4**)

$$b_1 + b_2 = \sqrt{(x_2 - x_1)^2 + (y_2 - y_1)^2} = d$$

(**Equation S5**)

The above equations can then be rearranged to form equations S6 and S7:

$$b_2^2 - b_1^2 = r_2^2 - r_1^2$$

(**Equation S6**)

$$(b_1 + b_2)^2 = d^2$$

(**Equation S7**)

Equations S6 and S7 can then be rearranged to form equation S8:

$$b_2 = \frac{r_2^2 - r_1^2 + d^2}{2d}$$

(**Equation S8**)

Equation S8 can then be combined with equation S4 and solved for *a* to give equation S9. Equation S9 can be solved using the experimentally obtained geometrical parameters to give a value for *a*.

$$a = \frac{1}{d}\sqrt{\left(4d^2 r_2^2\right) - (r_2^2 - r_1^2 + d^2)^2}$$

(**Equation S9**)

Equation S7 is then used with trigonometry to calculate the contact angle θ using the value of a obtained from equation S9 and the radii of one of the droplets. This is shown in equation S10. Figure S5 depicts the trigonometric relationship between the contact angle and the parameters used to calculate it.

$$\theta = 90 - \left(cos^{-1}\left(\frac{a/2}{r_1}\right)\frac{180}{\pi}\right)$$

(**Equation S10**)
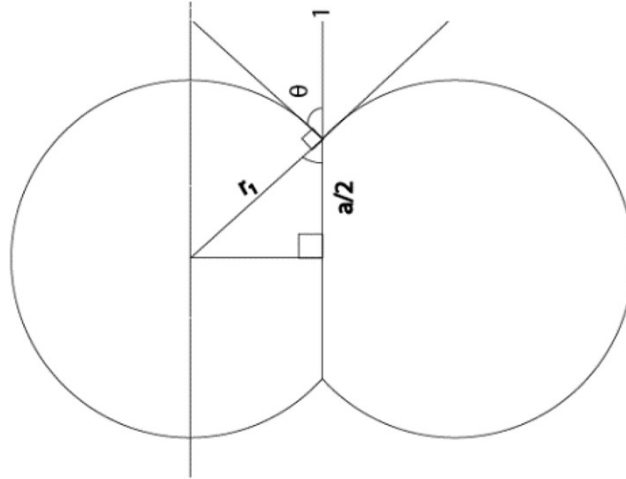
Figure S5: Schematic of the geometrical parameters utilised to find the DIB contact angle θ.

Calculating the bilayer surface tension

For asymmetric volume DIBs *Barlow et al.* showed that the bilayer surface tension (γ_b) could be given by equation S11[9]. Within the equation θ_1 and θ_2 are contact angles, θ_b is the angle relative to the x axis that balances the surface tensions and γ_2 is the surface tension of droplet 2. These geometrical properties are also indicated by figure S6. In the case of our structures, it is justified to use DIB equations as other microscale DIB systems[10] have found similar values to larger DIB systems.

$$\gamma_b = \gamma_2 \frac{\cot(\theta_1)\sin(\theta_2) + \cos(\theta_2)}{\cos(\theta_b) - \cos(\theta_1)\sin(\theta_b)}$$

(**Equation S11**)
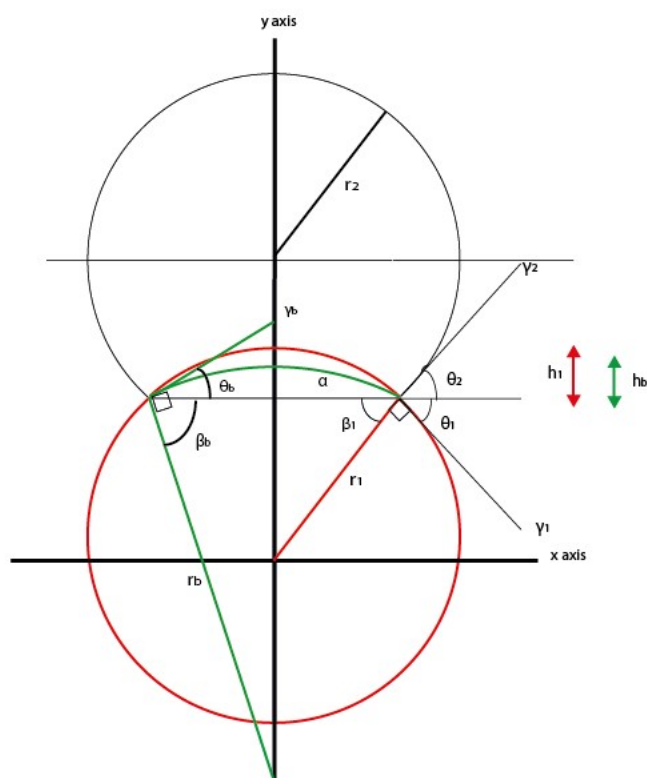
Figure S6: Adapted schematic from *Barlow et al.* [9] indicating the various geometrical parameters used to find the bilayer surface tension.

Barlow et al. also showed that taking into account θ_b for asymmetric volume DIBs gave a bilayer surface tension value which was within the error of the bilayer surface tension gathered through a simplified formula for symmetric DIB (where one of the assumptions is that the bilayer curvature can be ignored)[9]. This indicated that the bilayer curvature has only a small effect on the bilayer surface tension. As a result, to simplify the calculations required to find the bilayer surface tension, it was neglected for these calculations and treated as zero.

As a consequence, the only values required to calculate the bilayer surface tension were the contact angles θ_1 and θ_2 which can be readily obtained from the contact angle data and the surface tension of a constituent droplet (γ_2). From literature it could be seen that for a POPC monolayer this value was 0.80 mN m^{-1} [11]. As the trilayer structures are templated from vesicles that have significantly lower surface tensions (~10^{-3} mN m^{-1})[12,13] it can be assumed that the outer monolayer is dominating the surface tension energetics of the system. As a consequence, in all further calculations, it is assumed that the impact of the inner and central monolayers upon the trilayer droplet surface tension is negligible. Hence the monolayer surface tension for the trilayer droplets is taken as value of 0.8 mN m^{-1}.

By using equation S11 with all the parameters discussed above the bilayer surface tensions for the DIB systems could be calculated. The results for this are summarised within figure S7.
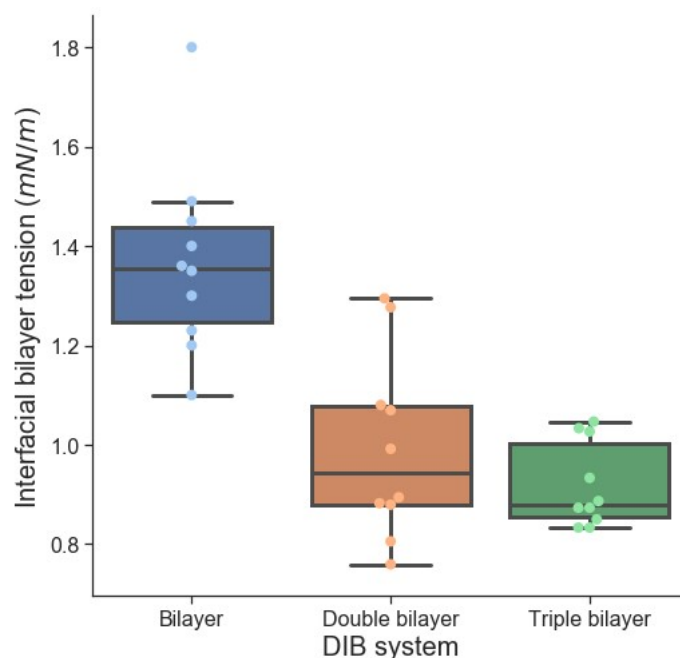
Figure S7: The interfacial bilayer tensions for asymmetric volume DIB systems comprised of monolayer and trilayer stabilised droplets (n=10). The box plots indicate the median and the interquartile range within the coloured region while the whiskers show the maximum/ minimum values (1.5x interquartile range); any values outside the whistlers are outliers.

This figure shows that the increasing number of bilayers decreases the bilayer interfacial tension. This could be occurring due to the additional lipid bilayers within the multi-DIBs providing a rigid hydrogen bonding network which stabilises the DIB interface and reduces the interfacial tension of the multi-membrane structure. The larger deviation of double bilayer interfacial tensions is thought to arise through the system being asymmetric in constituent droplet structure and volume thus producing a wider range of DIB conformations that will have different tension properties. The other DIB systems are only asymmetric in volume.

Calculating the adhesion energy

The adhesion energy values could be calculated through equation S12 where γ_m is the constituent droplet surface tension and θ is the contact angle[14]:

$$\Delta F = 2\gamma_m(1 - \cos(\theta))$$

(Equation S12)
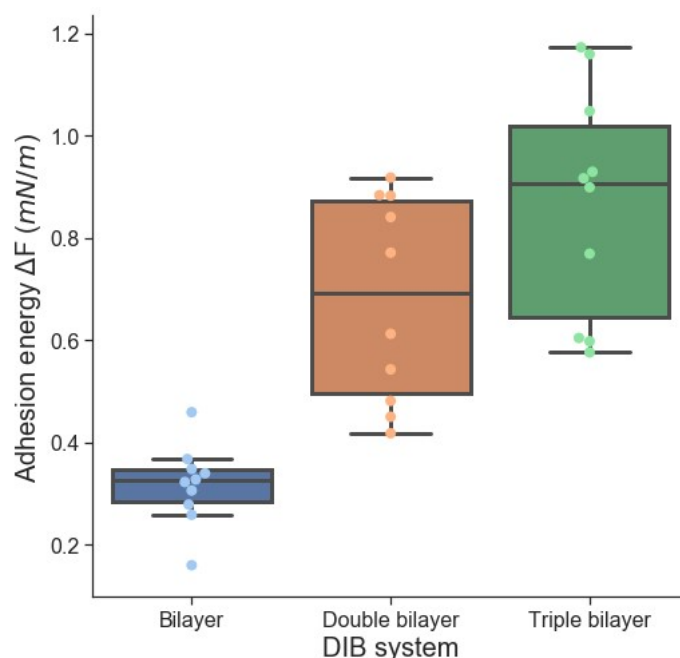
Figure S8: The adhesion energies for asymmetric volume DIB systems comprised of monolayer and trilayer stabilised droplets (n=10). The box plots indicate the median and the interquartile range within the coloured region while the whiskers show the maximum/ minimum values (1.5x interquartile range); any values outside the whistlers are outliers.

This analysis demonstrates that with increasing lamellarity there is an increase in adhesion energy. However, this becomes less pronounced as the number of bilayers increase. This indicates that the adhesion energy is heavily governed by the bilayer produced between the two droplets. The extra bilayers do however exert an influence on stabilising this interface which could arise from hydrogen bonding networks between aligning bilayers[15] although this influence wanes as the lamellarity increases.

The results from this calculation (and as a consequence the contact angle data) appear valid as the DIBs formed from POPC monolayer droplets have very similar adhesion energy values to DOPC and DPPC DIB systems in literature[16]. The DOPC and DPPC monolayer DIB's have adhesion energies of 0.29 and 0.28 mN m^{-1} respectively while the POPC monolayer DIB adhesion energy measured in this work has a mean value of 0.32 mN m^{-1}.

Acknowledgments

Author Contributions

MEA designed and performed experiments, wrote the manuscript, and carried out data analysis. JA conducted experiments and carried out data analysis. YE designed experiments and helped revise the manuscript.

References

1   A. Moga, N. Yandrapalli, R. Dimova and T. Robinson, *ChemBioChem*, 2019, **20**, 2674–2682.
2   T. Ip, Q. Li, N. Brooks and Y. Elani, *ChemBioChem*, 2021, **22**, 2275–2281.
3   V. Faugeras, O. Duclos, D. Bazile and A. R. Thiam, *Soft Matter*, 2020, **16**, 5970–5980.
4   S. Bachler, D. Haidas, M. Ort, T. A. Duncombe and P. S. Dittrich, *Commun. Biol.*, 2020, **3**, 1–9.
5   G. De Wit, J. S. H. Danial, P. Kukura and M. I. Wallace, *Proc. Natl. Acad. Sci. U. S. A.*, 2015, **112**, 12299–12303.
6   J. S. Najem, M. D. Dunlap, I. D. Rowe, E. C. Freeman, J. W. Grant, S. Sukharev and D. J. Leo, *Sci. Rep.*, 2015, **5**, 1–11.
7   N. E. Barlow, H. Kusumaatmaja, A. Salehi-Reyhani, N. Brooks, L. M. C. Barter, A. J. Flemming and O. Ces, *J. R. Soc. Interface*, 2018, **15**.
8   J. B. Boreyko, P. Mruetusatorn, S. A. Sarles, S. T. Retterer and C. P. Collier, *J. Am. Chem. Soc.*, 2013, **135**, 5545–5548.
9   G. A. Venkatesan, G. J. Taylor, C. M. Basham, N. G. Brady, C. P. Collier and S. A. Sarles, *Biomicrofluidics*, 2018, **12**, 024101.
10   J. O. Rädler, T. J. Feder, H. H. Strey and E. Sackmann, *Phys. Rev. E*, 1995, **51**, 4526–4536.
11   F. Jähnig, *Biophys. J.*, 1996, 71, 1348–1349.
12   M. P. Aronson and H. M. Princen, *Nature*, 1980, **286**, 370–372.
13   L. Tayebi, Y. Ma, D. Vashaee, G. Chen, S. K. Sinha and A. N. Parikh, *Nat. Mater.*, 2012, **11**, 1074–1080.
14   M. Yanagisawa, T. A. Yoshida, M. Furuta, S. Nakata and M. Tokita, *Soft Matter*, 2013, **9**, 5891–5897.